Properties of Potassium

T.G. Tiecke

van der Waals-Zeeman institute
University of Amsterdam
The Netherlands
v1.0 (February, 2010)

1 Introduction

This document is a stand-alone version of the appendix on potasssium properties of my thesis [1]. It is meant to provide an overview of the properties of atomic potassium useful for experiments on ultracold gases. A thorough review of the properties of lithium has been given in the thesis of Michael Gehm [2, 3]. For the other alkali atoms extended reviews have been given for Na, Rb and Cs by Daniel Steck [4].

2 General Properties

Potassium is an alkali-metal denoted by the chemical symbol K and atomic number $Z = 19$. It has been discovered in 1807 by deriving it from potassium hydroxide KOH. Being an alkali atom it has only one electron in the outermost shell and the charge of the nucleus is being shielded by the core electrons. This makes the element very chemically reactive due to the relatively low ionization energy of the outermost electron. The basic physical properties of potassium are listed in Table 2. Potassium has a vapor pressure given in mbar by [5]:

Mass number A	Neutrons N	Abundance (%) [6]	m (u) [8]	τ [9]	I [9]
39	20	93.2581(44)	38.96370668(20)	stable	3/2
40	21	0.0117(1)	39.96399848(21)	1.28×10^9 y	4
41	22	6.7302(44)	40.96182576(21)	stable	3/2

Table 1: Naturally occurring isotopes of potassium. The atomic number of potassium is $Z = 19$. The given properties are the atomic number A, the number of neutrons in the nucleus N, the abundance, the atomic mass m, the lifetime τ and the nuclear spin I.

Melting point	$63.65°C$ (336.8 K)	[10]
Boiling point	$774.0°C$ (1047.15 K)	[10]
Density at 293 K	0.862 g/cm^3	[10]
Ionization energy	418.8 kJ mol^{-1}	[10]
	4.34066345 eV	[11]
Vapor pressure at 293 K	1.3×10^{-8} mbar	[5]
Electronic structure	$1s^2 2s^2 p^6 3s^2 p^6 4s^1$	

Table 2: General properties of potassium

$$\begin{aligned} \text{(solid)} \qquad & \log\ p = 7.9667 - \frac{4646}{T} \qquad 298\ \text{K} < T < T_m. \\ \text{(liquid)} \qquad & \log\ p = 7.4077 - \frac{4453}{T} \qquad T_m < T < 600\ \text{K} \end{aligned} \tag{1}$$

Figure 1 depicts the vapor pressure over the valid range of Eq. 1.

Potassium has a chemical weight of 39.0983(1) [6] and appears naturally in three isotopes, ^{39}K, ^{40}K and ^{41}K which are listed in Table 1. The fermionic isotope ^{40}K has two radioactive decay channels. In 89% of the cases it decays through a β^- decay of 1.311MeV resulting in the stable ^{40}Ar. In the remaining 11% it decays through electron capture (K-capture) to ^{40}Ca [7]. The former decay channel is commonly used for dating of rocks.

3 Optical properties

The strongest spectral lines of the ground state potassium atom are the D1 ($^2S \rightarrow\ ^2P_{1/2}$) and D2 ($^2S \rightarrow\ ^2P_{3/2}$) lines. The most recent high precision measurements of the optical transition frequencies of potassium have been published by Falke *et al.* [12]. Tables 3 to 8 list the properties of the D1 and D2 lines for the various isotopes.

The natural lifetime τ of an excited state is related to the linewidth of the associated transition by

$$\Gamma = \frac{1}{\tau} \tag{2}$$

where Γ is the natural linewidth. A temperature can be related to this linewidth, which is referred to as the *Doppler temperature*

$$k_B T_D = \frac{\hbar \Gamma}{2}$$

where k_B is the Boltzmann constant. The wavenumber k and frequency ν of a transition are related to the wavelength λ by

$$k = \frac{2\pi}{\lambda}, \qquad \nu = \frac{c}{\lambda} \tag{3}$$

When an atom emits or absorbs a photon the momentum of the photon is transferred to the atom by the simple relation

$$m v_{rec} = \hbar k \tag{4}$$

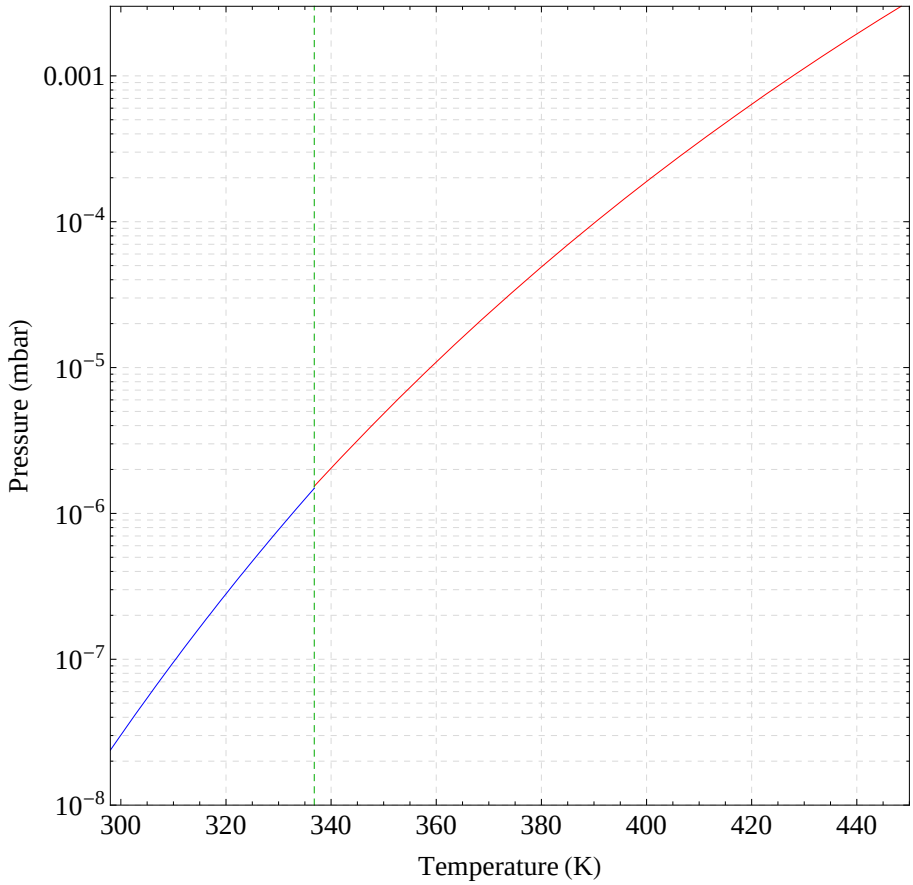

Figure 1: Vapor pressure of potassium taken from [5]. The green dashed line indicates the melting point of $T = 336.8°\mathrm{C}$.

Property	symbol	value	reference
Frequency	ν	389.286058716(62) THz	[12]
Wavelength	λ	770.108385049(123) nm	
Wavenumber	$k/2\pi$	12985.1851928(21) cm^{-1}	
Lifetime	τ	26.37(5) ns	[13]
Natural linewidth	$\Gamma/2\pi$	6.03(1) MHz	
Recoil velocity	v_{rec}	1.329825973(7) cm/s	
Recoil Temperature	T_{rec}	0.41436702 μK	
Doppler Temperature	T_D	145 μK	

Table 3: Optical properties of the ^{39}K D1-line.

Property	symbol	value	reference
Frequency	ν	391.01617003(12) THz	[12]
Wavelength	λ	766.700921822(24) nm	
Wavenumber	$k/2\pi$	13042.8954964(4) cm^{-1}	
Lifetime	τ	26.37(5) ns	[13]
Natural linewidth	$\Gamma/2\pi$	6.035(11) MHz	
Recoil velocity	v_{rec}	1.335736144(7) cm/s	
Recoil Temperature	T_{rec}	0.41805837 μK	
Doppler Temperature	T_D	145 μK	
Saturation intensity	I_s	1.75 mW/cm^2	

Table 4: Optical properties of the ^{39}K D2-line.

where m is the mass of the atom, v_{rec} is the recoil velocity obtained (lost) by the absorption (emission) process and $\hbar = h/2\pi$ is the reduced Planck constant. A temperature can be associated to this velocity, which is referred to as the recoil temperature

$$k_B T_{rec} = \frac{1}{2} m v_{rec}^2 \tag{5}$$

Finally, we can define a saturation intensity for a transition. This intensity is defined as the intensity where the optical Rabi-frequency equals the spontaneous decay rate. The optical Rabi-frequency depends on the properties of the transition, here we only give the expression for a cycling transition

$$I_s = \frac{\pi h c}{3\lambda^3 \tau}$$

4 Fine structure, Hyperfine structure and the Zeeman effect

The fine structure interaction originates from the coupling of the orbital angular momentum **L** of the valence electron and its spin **S** with corresponding quantum numbers L and S respectively. The total electronic angular momentum is given by:

Property	symbol	value	reference
Frequency	ν	389.286184353(73) THz	[12]
Wavelength	λ	770.108136507(144) nm	
Wavenumber	$k/2\pi$	12985.1893857(24) cm^{-1}	
Lifetime	τ	26.37(5) ns	[13]
Natural linewidth	$\Gamma/2\pi$	6.035(11) MHz	
Recoil velocity	v_{rec}	1.296541083(7) cm/s	
Recoil Temperature	T_{rec}	0.40399576 μK	
Doppler Temperature	T_D	145 μK	

Table 5: Optical properties of the ^{40}K D1-line.

Property	symbol	value	reference
Frequency	ν	391.016296050(88) THz	[12]
Wavelength	λ	766.700674872(173) nm	
Wavenumber	$k/2\pi$	13042.8997000(29) cm^{-1}	
Lifetime	τ	26.37(5) ns	[13]
Natural linewidth	$\Gamma/2\pi$	6.035(11) MHz	
Recoil velocity	v_{rec}	1.302303324(7) cm/s	
Recoil Temperature	T_{rec}	0.40399576 μK	
Doppler Temperature	T_D	145 μK	
Saturation intensity	I_s	1.75 $\mathrm{mW/cm}^2$	

Table 6: Optical properties of the ^{40}K D2-line.

Property	symbol	value	reference
Frequency	ν	389.286294205(62) THz	[12]
Wavelength	λ	770.107919192(123) nm	
Wavenumber	$k/2\pi$	12985.1930500(21) cm^{-1}	
Lifetime	τ	26.37(5) ns	[13]
Natural linewidth	$\Gamma/2\pi$	6.035(11) MHz	
Recoil velocity	v_{rec}	1.264957788(6) cm/s	
Recoil Temperature	T_{rec}	0.41408279 μK	
Doppler Temperature	T_D	145 μK	

Table 7: Optical properties of the ^{41}K D1-line.

Property	symbol	value	reference
Frequency	ν	391.01640621(12) THz	[12]
Wavelength	λ	766.70045870(2) nm	
Wavenumber	$k/2\pi$	13042.903375(1) cm^{-1}	
Lifetime	τ	26.37(5) ns	[13]
Natural linewidth	$\Gamma/2\pi$	6.035(11) MHz	
Recoil velocity	v_{rec}	1.2070579662(7) cm/s	
Recoil Temperature	T_{rec}	0.41408279 μK	
Doppler Temperature	T_D	145 μK	
Saturation intensity	I_s	1.75 $\mathrm{mW/cm}^2$	

Table 8: Optical properties of the ^{41}K D2-line.

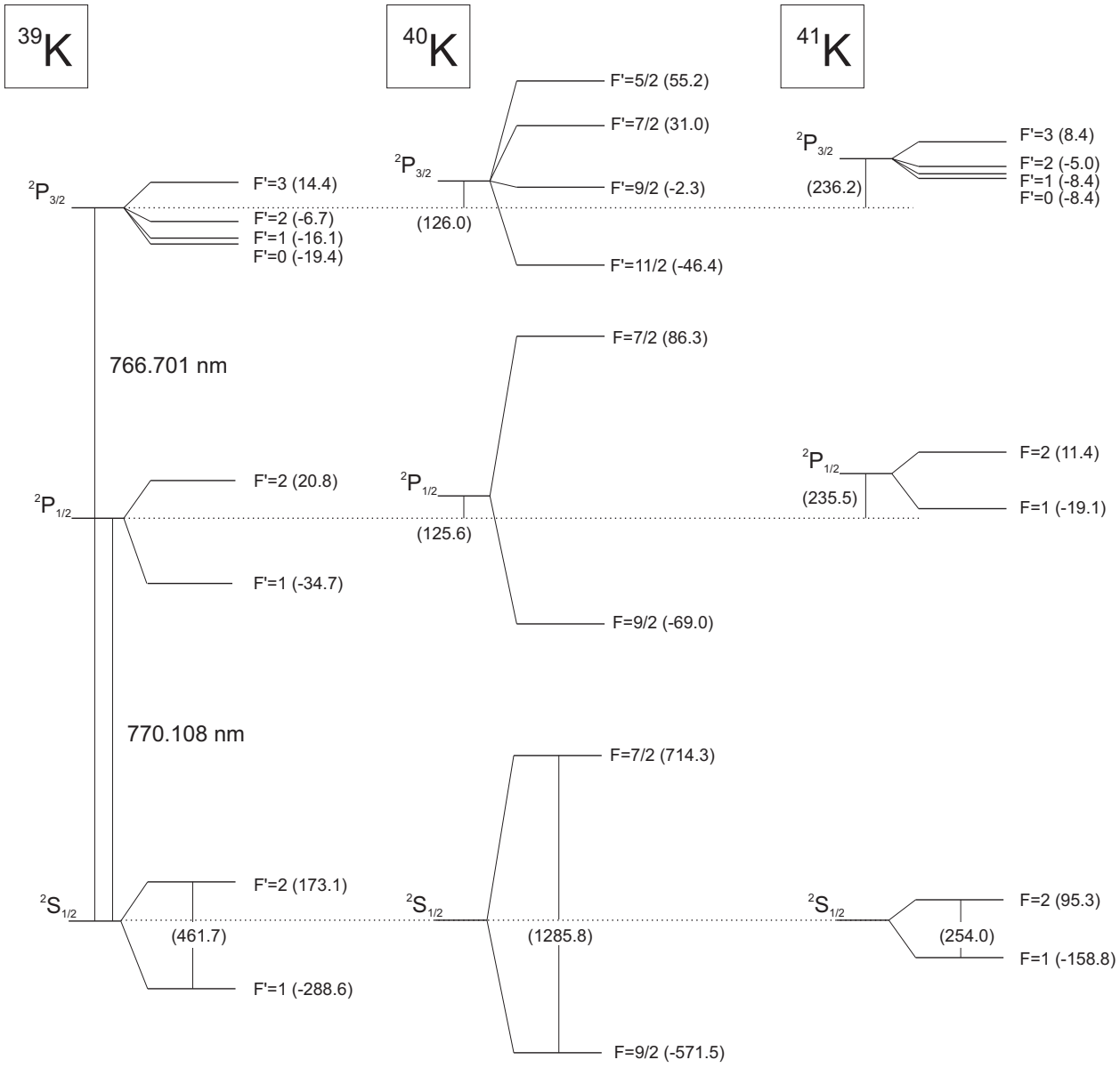

Figure 2: Optical transitions of the D1 and D2-lines of ^{39}K, ^{40}K and ^{41}K. A similar plot including ^{37}K, ^{38}K can be found in [9]. Numerical values are taken from [12] and [14]. Note the inverted hyperfine structure for ^{40}K.

$$\mathbf{J} = \mathbf{L} + \mathbf{S}$$

and the quantum number J associated with the operator $\mathbf{J}$ is in the range of $|L - S| \leq J \leq L + S$. The electronic ground state of ^{40}K is the $4^2S_{1/2}$ level, with $L = 0$ and $S = 1/2$, therefore $J = 1/2$. For the first excited state $L = 1$ and $S = 1/2$ therefore $J = 1/2$ or $J = 3/2$ corresponding to the states $4^2P_{1/2}$ and $4^2P_{3/2}$ respectively. The fine structure interaction lifts the degeneracy of the $4^2P_{1/2}$ and $4^2P_{3/2}$ levels, splitting the spectral lines in the D_1 line ($4^2S_{1/2} \rightarrow 4^2P_{1/2}$) and the D_2 line ($4^2S_{1/2} \rightarrow 4^2P_{3/2}$).

The hyperfine interaction originates from the coupling of the nuclear spin $\mathbf{I}$ with the total electronic angular momentum

$$\mathbf{F} = \mathbf{J} + \mathbf{I}$$

where the quantum number F associated with the operator $\mathbf{F}$ is in the range of $|J - I| \leq F \leq J + I$, where I is the quantum number corresponding to the operator $\mathbf{I}$. For ^{40}K the fine-structure splitting is $\Delta E_{FS} \simeq h \times 1.7$ THz, therefore the two excited states can be considered separately when considering smaller perturbations like the hyperfine or Zeeman interaction which are on the order of a few GHz or less.

The Hamiltonian describing the hyperfine structure for the two excited states described above is given by [14, 15]

$$\mathbf{H}^{\mathrm{hf}} = \frac{a_{hf}}{\hbar^2}\mathbf{I}\cdot\mathbf{J} + \frac{b_{hf}}{\hbar^2}\frac{3(\mathbf{I}\cdot\mathbf{J})^2 + \frac{3}{2}(\mathbf{I}\cdot\mathbf{J}) - \mathbf{I}^2\mathbf{J}^2}{2I(2I-1)J(2J-1)},$$

where a_{hf} and b_{hf} are the magnetic dipole and electric quadrupole constants respectively. The dot product is given by

$$\mathbf{I}\cdot\mathbf{J} = \frac{1}{2}(\mathbf{F}^2 - \mathbf{I}^2 - \mathbf{J}^2)$$

This hyperfine interaction lifts the spin degeneracy due to the different values of the total angular momentum F. The energy shift of the manifolds are given by

$$\delta E_{hf} = \frac{a_{hf}}{2}\left[F(F+1) - I(I+1) - J(J+1)\right]$$

For a $S = 1/2$ system in the electronic grounstate, $J = 1/2$, the energy splitting due to the hyperfine interaction in zero field is given by

$$\Delta E_{hf} = \frac{a_{hf}}{2}\left(I + \frac{1}{2}\right)$$

In the presence of an external magnetic field the Zeeman interaction has to be taken into account

$$\mathbf{H}^{\mathrm{Z}} = (\mu_B/\hbar)(g_J\mathbf{J} + g_I\mathbf{I})\cdot\mathbf{B},$$

where g_J is the Landé g-factor of the electron and g_I the nuclear gyromagnetic factor. Note that different sign conventions for g_I are used in literature, here we take the convention consistent with the common references in this context [14, 4, 3], such that $\mu = -g_I\mu_B\mathbf{I}$. The factor g_J can be written as

$$g_J = g_L\frac{J(J+1) - S(S+1) + L(L+1)}{2J(J+1)} + g_S\frac{J(J+1) + S(S+1) - L(L+1)}{2J(J+1)},$$

where g_S is the electron g-factor, g_L is the gyromagnetic factor of the orbital, given by $g_L = 1 - m_e/m_n$, where m_e is the electron mass and m_n is the nuclear mass. The total hyperfine interaction in the presence of an external magnetic field is now given by the internal hamiltonian

$$\mathbf{H}^{\mathrm{int}} = \mathbf{H}^{\mathrm{hf}} + \mathbf{H}^{\mathrm{Z}} \tag{6}$$

In the absence of orbital angular momentum, $L = 0$, and for $S = 1/2$, the eigenvalues of Eq. 6 correspond to the *Breit-Rabi formula* [16]

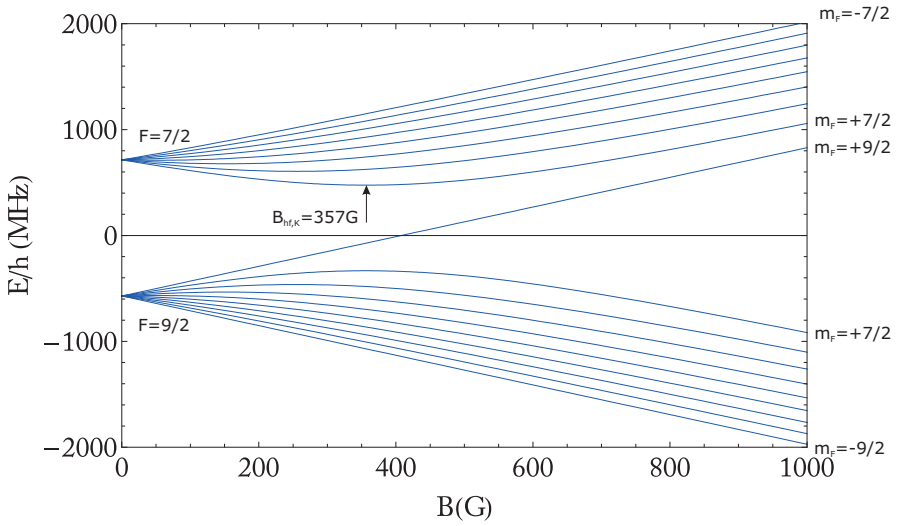

Figure 3: The hyperfine structure of the $^2S_{1/2}$ groundstate of ^{40}K. The states are labeled with their low-field quantum numbers $|F, m_F\rangle$. Note the inverted hyperfine structure.

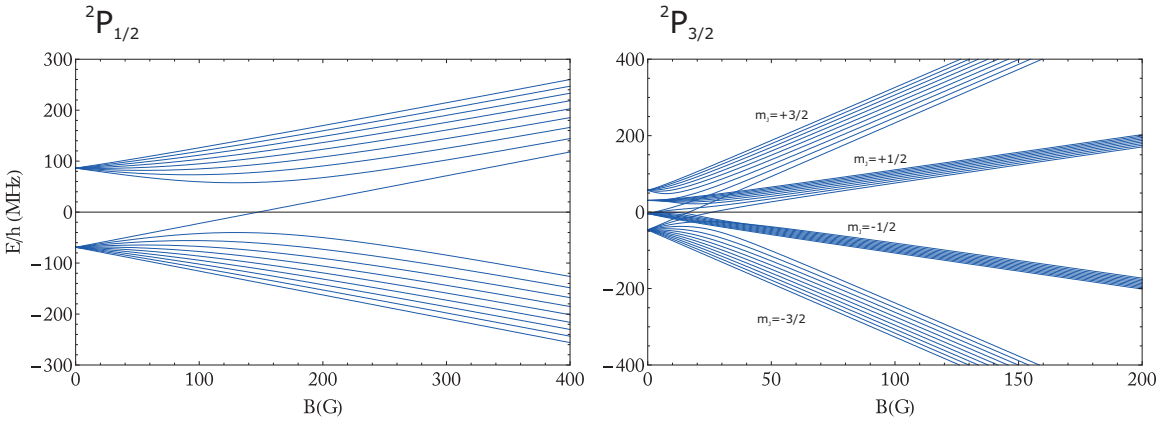

Figure 4: Hyperfine structure of the $^2P_{1/2}$ (D1) and the $^2P_{3/2}$ (D2) levels of ^{40}K.

$$E^{hf}(B) = -\frac{a^{hf}}{4} + g_I \mu_B m_f B \pm \frac{a^{hf}(I+1/2)}{2}\left(1 + \frac{4m_f x}{2I+1} + x^2\right)^{1/2} \tag{7}$$
$$x = \frac{(g_S - g_I)\mu_B}{a^{hf}(I+1/2)}B$$

where $\mu_B = 9.27400915 \times 10^{-24}$ JT^{-1} is the Bohr-magneton and the sign corresponds to the manifolds with $F = I \pm S$.

Figures 3 and 4 show the eigenvalues of Eq. 6 for the $^2S_{1/2}$ ground state and the $^2P_{1/2}$ and $^2P_{3/2}$ excited states of ^{40}K respectively.

4.1 Transition strengths

In this section we present the transition strengths for ^{40}K. We do not elaborate on the physics behind the transition dipole matrix elements. For a more thorough description and the transition strengths for ^{39}K and ^{41}K we refer to Ref. [18]. The transition matrix element coupling a ground state defined by the quantum numbers J, F, m_F to an excited state with quantum numbers J', F', m'_F is given by

Constant	symbol	^{39}K $h \times$ MHz	^{40}K $h \times$ MHz	^{41}K $h \times$ MHz	Ref.
$4p^2S_{1/2}$ magnetic dipole	a_{hf}	230.8598601(3)	−285.7308(24)	127.0069352(6)	[14]
$4p^2P_{1/2}$ magnetic dipole	a_{hf}	27.775(42)	−34.523(25)	15.245(42)	[12]
$4p^2P_{3/2}$ magnetic dipole	a_{hf}	6.093(25)	−7.585(10)	3.363(25)	[12]
$4p^2P_{3/2}$ electric quadrupole	b_{hf}	2.786(71)	−3.445(90)	3.351(71)	[12]

Table 9: Hyperfine structure coefficients for the ground state and the first exited state.

Property	Isotope	symbol	value	reference
Electron spin g-factor		g_S	2.0023193043622(15)	[17]
Total nuclear g-factor	^{39}K	g_I	−0.00014193489(12)	[14]
Total nuclear g-factor	^{40}K	g_I	+0.000176490(34)	[14]
Total nuclear g-factor	^{41}K	g_I	−0.00007790600(8)	[14]
Total electronic g-factor		$g_J(4p^2S_{1/2})$	2.00229421(24)	[14]
Total electronic g-factor		$g_J(4p^2P_{1/2})$	2/3	
Total electronic g-factor		$g_J(4p^2P_{3/2})$	4/3	

Table 10: Electronic and nuclear gyromagnetic factors. Experimental values for the g_J values are not available, therefore, we use the Russel-Saunders values which agree within the error margins for all other alkali atoms [14].

$$\mu_{eg} = e\langle J'F'm'_F|\hat{\varepsilon}\cdot\mathbf{r}|JFm_F\rangle$$

where e is the electronic charge, $\hat{\varepsilon}$ is the polarization unit vector of the optical electric field and $\mathbf{r}$ is the position operator. The transition strength is proportional to the square of the matrix element $D \sim |\mu_{eg}|^2$ and is given by

$$D \sim \left[\sqrt{(2J+1)(2J'+1)(2F+1)(2F'+1)}\begin{Bmatrix} L' & J' & S \\ J & L & 1 \end{Bmatrix}\begin{Bmatrix} J' & F' & I \\ F & J & 1 \end{Bmatrix}\begin{pmatrix} F & 1 & F' \\ m_F & q & -m'_F \end{pmatrix}\right]^2$$

where the curly brackets denote the Wigner-6j symbol, the normal bracket the Wigner 3j-symbol and $q = \pm 1$ for $\sigma^{\pm}$ polarized transitions and $q = 0$ for π transitions.

The relative strengths for the transitions D between different F, m_F values for ^{40}K are shown in Fig. 5 and 6 for σ^+ and π polarizations respectively. Transition strengths for σ^- can be obtained from Fig. 5 by replacing all m_F values with $-m_F$. The strengths are normalized to yield an integer value. Note that the normalizations are different for figures 5 and 6. Similar figures for ^{39}K and ^{41}K can be found in Ref. [18].

5 Scattering properties

The scattering properties of ultracold atoms are essential for the evaporative cooling processes and most experiments performed with ultracold gases. At typical densities temperatures the scattering reduces to s-wave scattering For ultracold scattering only lower partial waves play a role and the scattering properties are determined by the positions of only the last few bound states of the potentials. The scattering can be described by the radial Schrödinger equation

$$\left[-\frac{\hbar^2}{2\mu}\left(\frac{\partial^2}{\partial r^2} + \frac{2}{r}\frac{\partial}{\partial r} - \frac{l(l+1)}{r^2}\right) + V(r)\right]R(r) = \epsilon R(r), \tag{8}$$

where $R(r)$ is the radial wavefunction, l is the angular momentum quantum number and $V(r)$ is the scattering potential. Many ultracold scattering properties can be obtained with sufficient accuracy for general use in the lab by only using the accumulated phase method [19] and $V(r) = -C_6/r^6$. However, for Potassium accurate potentials have been published by Falke, *et al.* [20]. Because potassium has $S = 1/2$ the total spin of the potassium dimer can be either singlet ($S = 0$) or triplet ($S = 1$). Figure 7 shows the Born-Oppenheimer potentials for the singlet $X^1\Sigma$ and triplet $a^3\Sigma$ potentials. Solving Eq. 8

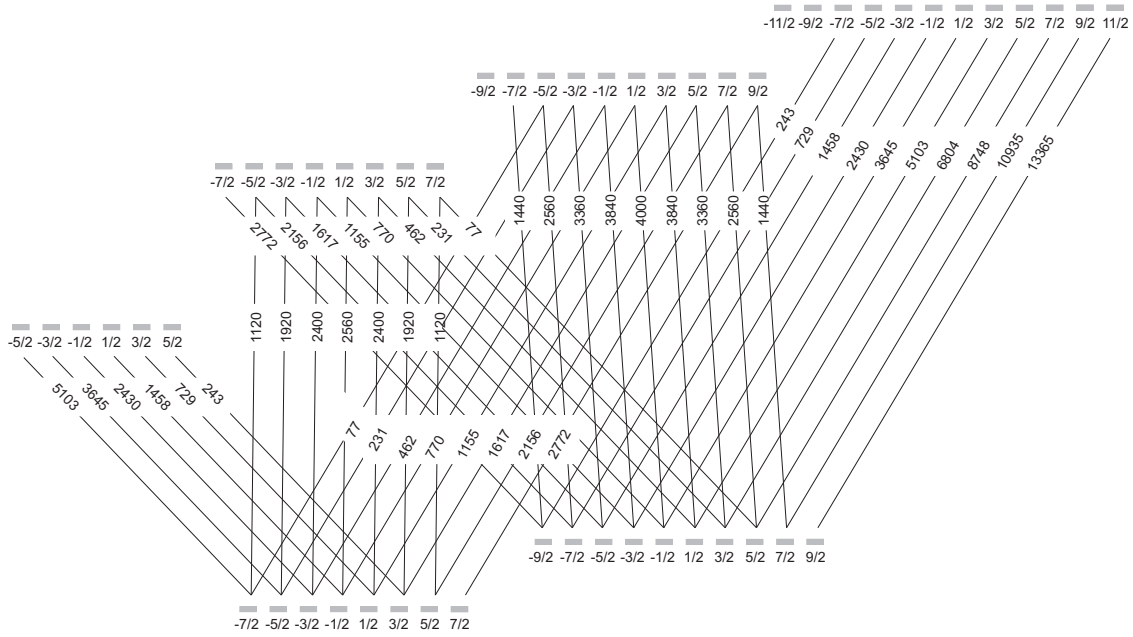

Figure 5: Transition probabilities for ^{40}K ($I = 4$) on σ^+ transitions, normalized to integer values.

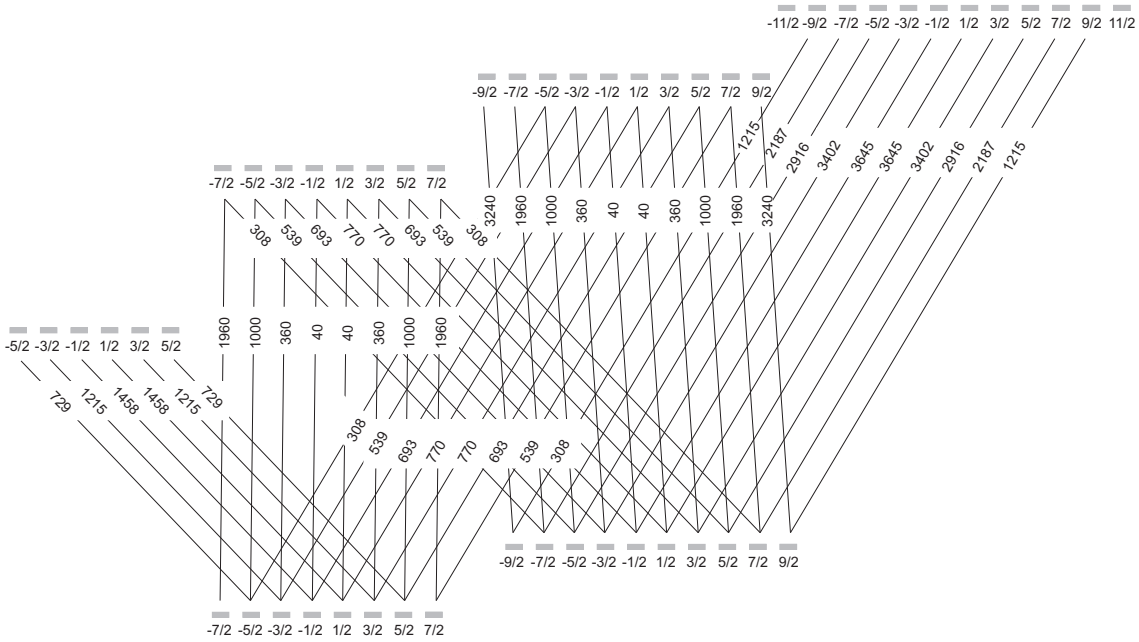

Figure 6: Transition probabilities for ^{40}K ($I = 4$) on π transitions, normalized to integer values.

isotope	a_s	a_t
39/39	138.49(12)	−33.48(18)
39/40	−2.84(10)	−1985(69)
39/41	113.07(12)	177.10(27)
40/40	104.41(9)	169.67(24)
40/41	−54.28(21)	97.39(9)
41/41	85.53(6)	60.54(6)

Table 11: s-wave scattering lengths for the various isotope-combinations of potassium, values are taken from Ref. [20]

	value	units
C_6	3925.9	$E_h a_0^6$
C_8	4.224×10^5	$E_h a_0^8$
C_{10}	4.938×10^7	$E_h a_0^{10}$
r_0 (^{39}K)	64.61	a_0
r_0 (^{40}K)	65.02	a_0
r_0 (^{41}K)	65.42	a_0

Table 12: Van der Waals properties of the scattering potential of potassium. $V_{vdw}(r) = -C_6/r^6 - C_8/r^8 - C_8/r^8$.

for $\epsilon \downarrow 0$ one can obtain the scattering length. Table 11 lists the s-wave scattering lengths of the various potassium isotopes [20].

To qualitatively describe the scattering for ^{40}K we compare the scattering lengths to the the van der Waals range. The van der Waals range is a measure for the typical range of the potential for an atomic species. It is defined as the range where the kinetic energy of confinement in the potential equals the potential energy and is given by [21]

$$r_0 = \frac{1}{2}\left(\frac{2\mu C_6}{\hbar^2}\right)^{1/4}$$

Using the van der Waals coefficient of $C_6 = 3925.9\ \mathrm{E}_h\mathrm{a}_0^6$ [20] for ^{40}K we obtain a van der Waals range of $r_0 \simeq 65\ \mathrm{a}_0$. The scattering lengths of both the singlet and triplet potentials are much larger than r_0 indicating resonant scattering due to the presence of a weakly bound state in both the singlet and triplet scattering potentials. Figure 8 shows the wavefunctions of the least bound states in the singlet and triplet potentials for ^{40}K. Note the horizontal logarithmic scale. The wavefunctions extend far into the asymptotic van der Waals tail of the potentials.

5.1 Feshbach resonances

The use of Feshbach resonances are essential for the study of ultracold gases, in particular for fermionic isotopes. A Feshbach resonance occurs due to a resonant coupling of a scattering pair of atoms with an energetically closed molecular state. The s-wave scattering length a in the vicinity of a Feshbach resonance is parameterized by

$$a(B) = a_{bg}\left(1 - \frac{\Delta B}{B - B_0}\right)$$

where a_{bg} is the background scattering length in absence of coupling to the molecular state, B_0 is the resonance position and ΔB is the magnetic field width of the resonance. Due to the resonant scattering in the open channels (i.e. a large background scattering length) the Feshbach resonances of ^{40}K have a broad character. For ^{39}K eight resonances have been experimentally obtained and are listed together with some theoretical predictions in table 13. For ^{40}K two experimentally characterized s-wave Feshbach resonances and one p-wave resonance have been published. The resonances are summarized in Table 14.

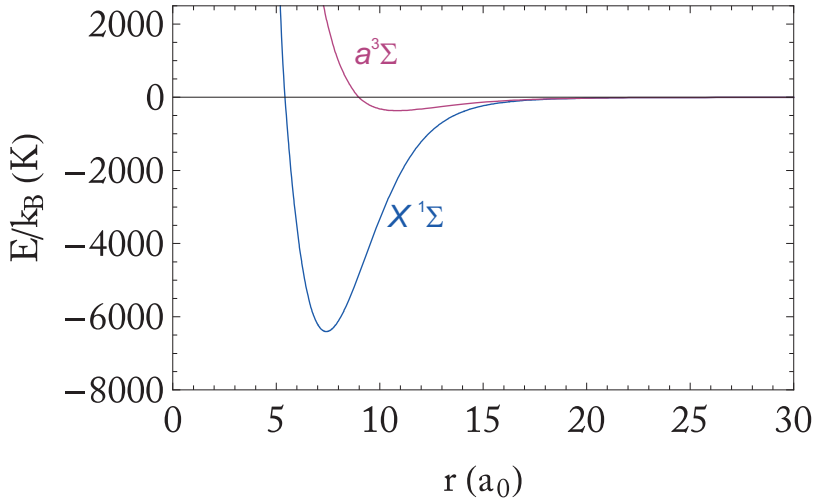

Figure 7: Born-Oppenheimer potentials $V_S(r)$ for the singlet $S = 0$, $X^1\Sigma$ and the triplet $S = 1$, $a^3\Sigma$ states.

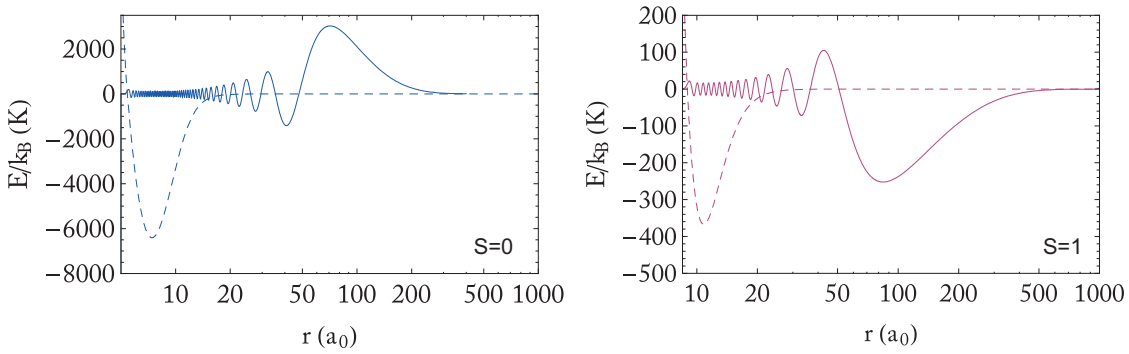

Figure 8: Wavefunctions of the least bound states of ^{40}K for the singlet (left) and triplet (right) potentials. The dashed curve indicates the potential and the solid curve the radial wavefunction of the least-bound vibrational levels. Note the horizontal logarithmic scale and the asymptotic character of the wavefunctions.

m_{f_1}, m_{f2}	B_0 (G)	$-\Delta B$ (G)	a_{bg} (a_0)
1 + 1	25.85 ± 0.1	0.47	−33
	403.4 ± 0.7	52	−29
	(745.1)	0.4	−35
	752.3 ± 0.1	0.4	−35
0 + 0	59.3 ± 0.6	9.6	−18
	66.0 ± 0.9	7.9	−18
	(471)	72	−28
	(490)	5	−28
	(825)	0.032	−36
	(832)	0.52	−36
-1 + -1	32.6 ± 1.5	−55	−19
	162.8 ± 0.9	37	−19
	562.2 ± 1.5	56	−29

Table 13: All published Feshbach resonances for ^{39}K. Numbers in brackets are only theoretically predicted. All values have been taken from Ref. [22]

m_{f_1}, m_{f2}	s/p	B_0 (G)	ΔB (G)	Ref.
-9/2 + -7/2	s	202.10 ± 0.07	7.8 ± 0.6	[23, 24, 25]
-9/2 + -5/2	s	224.21 ± 0.05	9.7 ± 0.6	[23, 26]
-7/2 + -7/2	p	~ 198.8		[23, 24, 27]

Table 14: All resonances are between spin states in the $F = 9/2$ manifold. This table has been adapted from Ref. [23]

References

[1] Tobias Gerard Tiecke. *Feshbach resonances in ultracold mixtures of the fermionic quantum gases 6Li and 40K*. PhD thesis, University of Amsterdam, 2009.

[2] M. E. Gehm. *Preparation of an Optically-Trapped Degenerate Fermi Gas of 6Li: Finding the Route to Degeneracy*. PhD thesis, Duke University, 2003.

[3] Michael Gehm. Properties of Lithium. http://www.phy.duke.edu/research/photon/ qoptics/techdocs/pdf/PropertiesOfLi.pdf.

[4] Daniel Steck. Alkali D Line Data. http://steck.us/alkalidata/.

[5] C. B. Alcock, V. P. Itkin, and M. K. Horrigan. Vapor pressure equations for the metallic elements: 298-2500K. *Canadian Metallurgical Quarterly*, 23:309, 1984.

[6] NIST Atomic Weigths and Isotopic Compositions. http://physics.nist.gov/PhysRefData/Compositions/index.ht

[7] A. Azman, A. Moljk, and J. Pahor. Electron Capture in Potassium 40. *Zeitschrift ffir Physik*, 208:234–237, 1968.

[8] G. Audi, A. H. Wapstra, and C. Thibault. The 2003 atomic mass evaluation: (II). Tables, graphs and references. *Nuclear Physics A*, 729(1):337 – 676, 2003. The 2003 NUBASE and Atomic Mass Evaluations.

[9] Robert Sylvester Williamson. Magneto-optical trapping of potassium isotopes. 1997.

[10] Chemical properties of the elements. http://www.chemicalelements.com/elements/k.html.

[11] NIST Atomic Spectra Database http://physics.nist.gov/PhysRefData/ASD/index.html.

[12] Stephan Falke, Eberhard Tiemann, Christian Lisdat, Harald Schnatz, and Gesine Grosche. Transition frequencies of the D lines of ^{39}K, ^{40}K, and ^{41}K measured with a femtosecond laser frequency comb. *Physical Review A (Atomic, Molecular, and Optical Physics)*, 74(3):032503, 2006.

[13] H. Wang, P. L. Gould, and W. C. Stwalley. Long-range interaction of the ^{39}K(4s)+^{39}K(4p) asymptote by photoassociative spectroscopy. I. The 0_g^- pure long-range state and the long-range potential constants. *The Journal of Chemical Physics*, 106(19):7899–7912, 1997.

[14] E. Arimondo, M. Inguscio, and P. Violino. Experimental determinations of the hyperfine structure in the alkali atoms. *Rev. Mod. Phys.*, 49(1):31–75, Jan 1977.

[15] Mitchel Weissbluth. *Atoms and Molecules*. Academic Press, 1980.

[16] G. Breit and I. I. Rabi. Measurement of Nuclear Spin. *Phys. Rev.*, 38(11):2082–2083, Dec 1931.

[17] Peter J. Mohr, Barry N. Taylor, and David B. Newell. CODATA recommended values of the fundamental physical constants: 2006. *Rev. Mod. Phys.*, 80(2):633–730, Jun 2008.

[18] H. Metcalf and P. van der Straten. *Laser Cooling and Trapping*. Springer, 1999.

[19] B. J. Verhaar, E. G. M. van Kempen, and S. J. J. M. F. Kokkelmans. Predicting scattering properties of ultracold atoms: Adiabatic accumulated phase method and mass scaling. *Physical Review A (Atomic, Molecular, and Optical Physics)*, 79(3):032711, 2009.

[20] Stephan Falke, Horst Knöckel, Jan Friebe, Matthias Riedmann, Eberhard Tiemann, and Christian Lisdat. Potassium ground-state scattering parameters and Born-Oppenheimer potentials from molecular spectroscopy. *Physical Review A (Atomic, Molecular, and Optical Physics)*, 78(1):012503, 2008.

[21] C. Chin, R. Grimm, Julienne, and E. P. S., Tiesinga. Feshbach Resonances in Ultracold Gases. *arxiv*, 2008.

[22] Chiara D'Errico, Matteo Zaccanti, Marco Fattori, Giacomo Roati, Massimo Inguscio, Giovanni Modugno, and Andrea Simoni. Feshbach resonances in ultracold 39K. *New Journal of Physics*, 9(7):223, 2007.

[23] Cindy Regal. *Experimental realization of BCS-BEC crossover physics with a Fermi gas of atoms*. PhD thesis, University of Colorado, 2005.

[24] C. A. Regal, C. Ticknor, J. L. Bohn, and D. S. Jin. Tuning p-Wave Interactions in an Ultracold Fermi Gas of Atoms. *Phys. Rev. Lett.*, 90(5):053201, Feb 2003.

[25] C. A. Regal, M. Greiner, and D. S. Jin. Observation of Resonance Condensation of Fermionic Atom Pairs. *Phys. Rev. Lett.*, 92(4):040403, Jan 2004.

[26] C. A. Regal and D. S. Jin. Measurement of Positive and Negative Scattering Lengths in a Fermi Gas of Atoms. *Phys. Rev. Lett.*, 90(23):230404, Jun 2003.

[27] C. Ticknor, C. A. Regal, D. S. Jin, and J. L. Bohn. Multiplet structure of Feshbach resonances in nonzero partial waves. *Phys. Rev. A*, 69(4):042712, Apr 2004.